Journal of Thermal Analysis and Calorimetry, Vol. 79 (2005) 579–585

SMECTIC ORDERING IN POLYMER LIQUID CRYSTAL-SILICA AEROGEL NANOCOMPOSITES
Studies of DSC and SAXS

Nádya Pesce da Silveira[1*], *F. Ehrburger-Dolle*[2], *C. Rochas*[2], *A. Rigacci*[3], *F. Vargas Pereira*[1] *and H. Westfahl Jr.*[4]

[1]Universidade Federal do Rio Grande do Sul, Instituto de Química, Av. Bento Gonçalves 9500 Porto Alegre - Rio Grande do Sul, CEP 91501 970 Caixa Postal 15003, Brazil
[2]Laboratoire de Spectrométrie Physique, UMR 5588 CNRS-UJF, 38402 Saint-Martin d'Hères, France
[3]CENERG, CEP, École des Mines de Paris, BP 207, 06904 Sophia-Antipolis, France
[4]Laboratório Nacional de Luz Síncrotron, Campinas, Brazil

Two series of side chain liquid crystal (SCLC) polyacrylate-silica aerogel nanocomposites have been investigated by small-angle X-ray scattering (SAXS) and differential scanning calorimetry (DSC). The first series (*ex-situ* nanocomposite) was obtained by infiltration of a smectic SCLC polyacrylate prepared by polymerisation in solution into monolithic aerogel slabs. The second one (*in-situ* nanocomposite) was prepared by photopolymerisation of the monomer infiltrated in the aerogel. The results are compared with those obtained for bulk polyacrylates. It is shown that the smectic ordering is not destroyed by confinement in the aerogel. Spacing of the smectic layers and smectic correlation lengths were deduced from the fit of the SAXS profiles to a Lorentzian function with a quadratic correction. The principal results suggest that *in-situ* polymerisation enhances the degree of order and the stability of the smectic phase in the nanocomposite.

Keywords: *aerogel-based nanocomposites, DSC, SAXS, side chain liquid crystal polymer, silica aerogel*

Introduction

Considerable attention has been paid in the last ten years to the study of thermotropic liquid crystals (LC) confined in porous solids [1]. In the field of fundamental research, liquid crystals embedded in complex geometries allow investigation of random disorder effects on physical systems; in the field of applied research, such composite materials are studied because of their interest for electro-optical applications [1]. Depending on the mesophase behaviour, the pore walls can either align the liquid crystals through surface anchoring or induce quenched disorder. Monolithic silica aerogels are generally used for LC confinement, although several papers are dealing with liquid crystals embedded in a network of pyrogenic silica aggregates [2 and references therein]. Silica aerogels possess a wide variety of exceptional properties, hence a striking number of applications particularly in optics or energetics [3]. At low densities, silica aerogels consist of a network of fractal aggregates and display a wide distribution of pore sizes [4, 5]. At higher densities, pores are smaller and the pore size distribution becomes narrower. It follows that the effect of pore sizes on the physical properties of liquid crystals can be investigated very precisely using silica aerogel. Up to now, confinement of LC was limited to low molecular mass nematogenics among others, octylcyanobiphenyl LC (8CB). To the best of our knowledge, no investigation dealing with confinement of liquid crystal polymers, or, more precisely, side chain liquid crystal (SCLC) polymers have been reported so far. In SCLC polymers [6], the mesogenic moities are attached to the polymer chain by a flexible spacer. Thus, the polymer chain imposes an alignment that can be improved by external electric or magnetic fields [7]. These molecules which combine the self-organising properties of liquid crystals with the structural advantages of polymers are interesting for applications like displays. Changing the chemical composition and the spacer length allows modification of the LC phase behaviour; confinement of these SCLC polymers in aerogels with different pore sizes is expected to yield a wide variety of nanocomposite materials displaying well defined characteristics. Furthermore, investigation of SCLC polymers in aerogels allows information not only in the field of their optical and dielectric properties but also in the field of polymers confined in porous networks [8, 9].

* Author for correspondence: nadya@iq.ufrgs.br

1388–6150/$20.00

Akadémiai Kiadó, Budapest, Hungary
Springer, Dordrecht, The Netherlands

The aim of the present work is to measure and analyse the phase behaviour of a chiral side chain acrylate polymer in bulk (POA) and confined in a silica aerogel (PIA). Because infiltration of large molecular size polymers in the aerogel porous network may be difficult, *in-situ* UV photopolymerisation of the monomer precursor is achieved [10]. The behaviour of the resulting nanocomposite (PPIA) is compared to that of the polymer photopolymerised in bulk, out of aerogel (PPOA) and to that of POA and PIA samples, for which polymerisation is achieved in solution. The phase transition temperature is determined by means of differential scanning calorimetry (DSC). Structure of the liquid crystal phase is investigated by means of small-angle X-ray scattering (SAXS) measurements performed in isothermal conditions.

Experimental

The starting chiral acrylate monomer [11] has a spacer containing eleven carbons, as represented in Fig. 1. Exhibiting only a crystal melting endotherm as probed by DSC, it is non-mesogenic. Bulk SCLC polyacrylates are obtained by two different methods: a) polymerisation of the monomer in a solution of toluene with AIBN (5 mass%) as initiator [11] (sample POA) and b) photo-initiated free-radical polymerisation of the monomer (sample PPOA). To prepare the PPOA sample, 3 mass% of 2,2-dimethoxy-1,2-diphenylethane-1-one (Irgacure 651) kindly provided by Ciba Speciality Chemicals Inc., and 50 ppm of *p*-methoxyphenol (Aldrich) to prevent thermal polymerisation are added to the monomer. Photopolymerisation is performed with an UV source (Oriel Instruments). The UV intensity, adjusted by changing the distance between the sample and the lamp, is 0.80 mW cm^{-2} at 365 nm. The sample is maintained slightly above the isotropic temperature of the monomer during the polymerisation procedure. In order to remove dissolved oxygen, the monomer to be photopolymerised is stored in the sample holders under nitrogen atmosphere (<2 ppm of oxygen). A high monomer conversion, checked by SAXS, is observed after 30 s of UV-irradiation.

Silica gels are synthesised in ethylacetoacetate by HF-catalysed polymerisation of H_2SO_4 pre-polymerised TEOS precursors. The monolithic silica aerogel (ρ=0.18±0.02 g cm^{-3}) is obtained by supercritical CO_2 drying of gels as described elsewhere [12]. It consists of a network of fractal aggregates (D_f=1.7±0.1) [4].

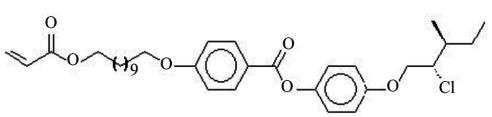

Fig. 1 General chemical structure of the chiral acrylate monomer

The aggregates are built by nanosize particles (less than 30 Å in diameter) with a smooth surface. The aerogel porosity ($\varnothing$=0.92±0.08) results from two families of pores: intra-aggregate pores characterized by a distribution peaking at nearly 80 Å and inter-aggregate voids characterized by a broad distribution of sizes up to about 800 Å [4]. The total pore volume V_p is 5.1±0.5 cm^3 g^{-1}.

Impregnation of the aerogel is performed as follows. A slab of aerogel (1.5 mm thick) and POA (or monomer) are separately heated to the isotropic temperature (T=337 K). The aerogel slab is then placed on the surface of the liquid under reduced pressure (0.16 atm). The impregnation of the aerogel by the liquid proceeds by capillary forces and complete filling is determined visually. The surface of the slab is lightly wiped up with filter paper to reduce superficial excess of bulk material and the PIA composite is ready for analysis. Opacification of the aerogel occurs immediately after filling. The mass of sample in the aerogel is of 0.20 g cm^{-3} for the polymer and 0.54 g cm^{-3} for the monomer.

DSC measurements are performed with a Perkin Elmer DSC2 apparatus. Heating and cooling scan rates of 10 K min^{-1} are used. In order to initialise the thermal history of the samples, two heating-cooling cycles are carried out. Transition temperatures are determined at the maximum of the endothermic peaks during the second heating scan.

The POA polyacrylate, used as a reference, changes from the crystalline to the mesophase. The nature of the mesophase was assigned as a smectic phase (*Sm*) with blurred Schlieren texture, as observed by optical microscopy [11].

SAXS measurements are performed on the French CRG beamline D2AM at the European Synchrotron Radiation Facility (ESRF), Grenoble, France [13]. The incident energy is 16.2 keV. An indirect illumination CCD detector (Princeton Instruments) is located at 27.5 cm from the sample. The scattering curve $I(q)$ is determined over a domain of q values ranging between $2\cdot10^{-3}$ and 0.8 $Å^{-1}$. The aerogel-SCLC polymer composites are placed in stainless steel sample holders closed by two mica windows (20 μm) and bulk polymers, in Lindemann capillaries (1.5 mm diameter). Sample holders or capillaries are mounted on a thermostatically controlled sample changer built on alluminium. Eleven temperatures ranging between 299 and 346 K were selected. At each temperature step, several minutes are allowed for temperature equilibrium before starting SAXS measurements. The whole procedure is fully automatic. The scattering intensity is corrected for the detector response and distortion, dark current signals, as well as sample transmission and background scattering.

Results and discussion

DSC curves from the four different samples POA, PIA, PPOA and PPIA, are plotted in Fig. 2. All samples show a dominant peak assigned to the crystal state (*K*)→smectic (*Sm*) phase transition and a weaker and broader one associated with the smectic (*Sm*)→sotropic (*I*) liquid-phase transition. The corresponding transition temperatures are indicated in Table 1. Transition temperatures are determined taking the second heating scan into account.

Table 1 Transition temperatures (*T*/K) of the SCLC polyacrylates determined by DSC; *K*=crystal state, *Sm*=smectic phase, *I*=isotropic liquid

	M_n	M_w/M_n	*K*	*Sm*	*I*
POA	21200	1.60	• 310	• 337	•
PIA	21200	1.60	• 306	• 333	•
PPOA	*	*	• 310	• *	•
PPIA	*	*	• 303	• 334	•

M_n– Molecular mass determined by size exclusion chromatography (SEC); * Not determined.

For the bulk SCLC polyacrylate (sample POA, Fig. 2, curve a) the phase transitions yield relatively well defined peaks, as expected. When the polymer is confined in aerogel (PIA, Fig. 2, curve c), the two peaks (corresponding to the *K*→*Sm* and the *Sm*→*I* transitions) shift to a lower temperature and become broader as a result of the pore size distribution in the silica aerogel. It is notable that the typical phase transitions of POA are maintained after confinement (PIA sample).

For the bulk polymer photopolymerised outside the aerogel (PPOA, Fig. 2, curve b), the *K*→*Sm* peak becomes broader, but located at the same temperature as POA. The *Sm*→*I* peak is very broad, as can be better seen on the second cooling curve. Since PPOA consists of a polymeric network where the cross-links between the main chains are formed by uniaxially oriented mesogenic units, a thermal stability of the ordering in the mesophase is expected [14]. As a consequence, the *Sm*→*I* phase transition gives a very small peak in the DSC curves [14]. In this case it is not possible to determine the temperature transition by means of DSC. Similarly, for PPIA (Fig, 2, curve d) that has been prepared by UV polymerisation inside the aerogel, the *Sm*→*I* peak is hardly seen on the second heating scan, and can be also better observed in the second cooling scan.

The major difference between PPOA (Fig. 2, curve b) and PPIA (Fig. 2, curve d) concerns the *K*→*Sm* transition for PPIA, that splits into two peaks in the second heating scan. The first one is located around 303 K, as encountered for PIA (confined POA). It is likely that, as for PIA, the temperature shift results from the confining pore sizes. For the second peak, $T_{K\rightarrow Sm}$ is close to that observed for the bulk polymers. It is tempting to assume that part of monomer is filling pores that are large enough to allow the same photopolymerization effect as in bulk. Another explanation would be the existence of unreacted monomer (Fig. 2, curve e) that exhibits a $T_{K\rightarrow I}$ around 310 K. For the monomer, the exothermal peak (288 K) followed by an endothermic peak (306 K) may be attributed to overcooling effects.

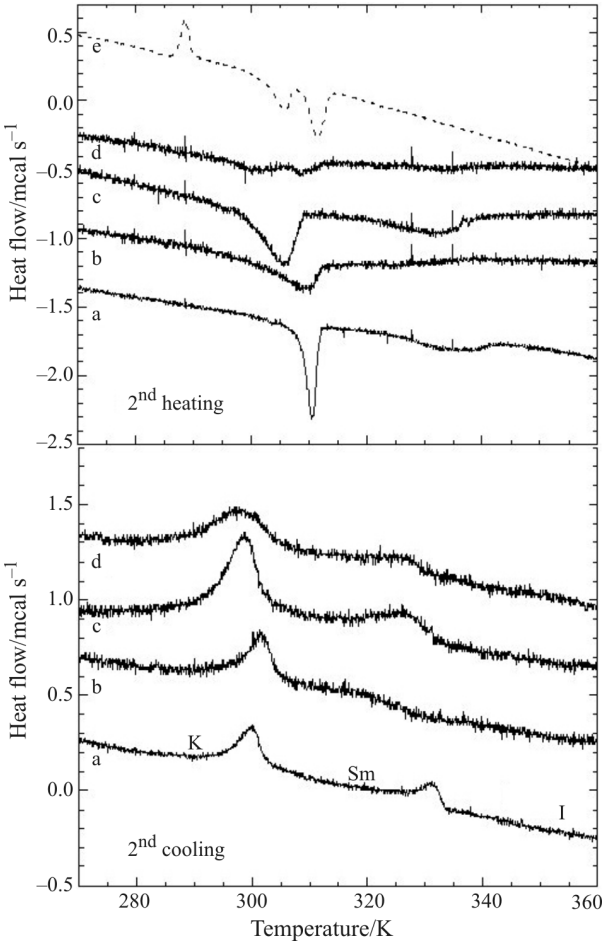

Fig. 2 DSC curves: a – SCLC polyacrylate prepared by polymerisation in solution (POA), b – SCLC polyacrylate photopolymerised in bulk (PPOA), c – SCLC polyacrylate confined in the aerogel (PIA), d – SCLC polyacrylate photopolymerised inside the aerogel (PPIA), e – monomer acrylate (the exothermal peak at 288 K followed by an endothermic peak at 306 K that are not observed during first heating could reveal overcooling effects)

The most important information obtained by DSC concerns the *K*→*Sm* phase transition. It is very similar for samples POA and PPOA (bulk polymers) and shows the same trends for both PIA and PPIA (confined polymers). Thus, it can be concluded that the smectic ordering temperature $T_{K\rightarrow Sm}$ depends more on confinement than on the method of monomer polymerisation. Confinement seems also to shift the temperature domain of the smectic phase to lower

temperatures. Information about the phase structure of the polymers in the samples is obtained by SAXS, as presented below.

Temperature-dependent SAXS curves obtained for the four samples are given in Figs 3 and 4. For PIA and PPIA, the background from aerogel scattering must be subtracted. The SAXS curve for the confined monomer measured at 346 K before photopolymerisation (isotropic liquid) is used as background.

The typical crystal state (*K*)→smectic phase (*Sm*) transition of sample POA can be observed in Fig. 3a, from the disappearance of the two peaks located at q=0.199 and 0.330 Å^{-1}, (299 and 303 K) and the appearance, at 308 K, of two new peaks at q=0.174 and 0.350 Å^{-1} (observed up to 338 K). The coexistence of *K* and *Sm* phases can be observed at 308 K. The corresponding *d* spacing in the smectic arrangement (d=2π/q) decreases slightly from 36.0 to 35.3 Å on increasing the temperature between 308 and 333 K as a result of the smectic modulation in the polymer. The 2-dimensional scattering images, not depicted here, show a circle of nearly uniform intensity. This feature indicates that the smectic layers are formed with no preferred direction. The second order

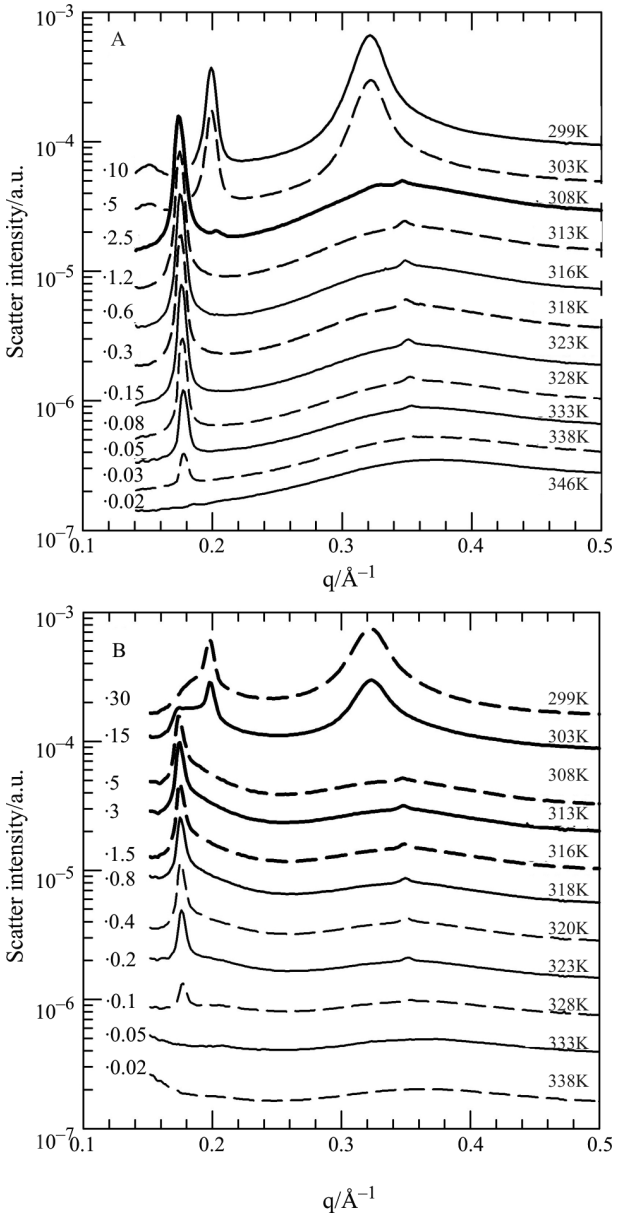

Fig. 3 SAXS profiles determined at different temperatures: a – SCLC polyacrylate (POA) prepared by polymerisation in solution; b – SCLC polyacrylate confined in aerogel (PIA) after subtraction of the aerogel scattering background

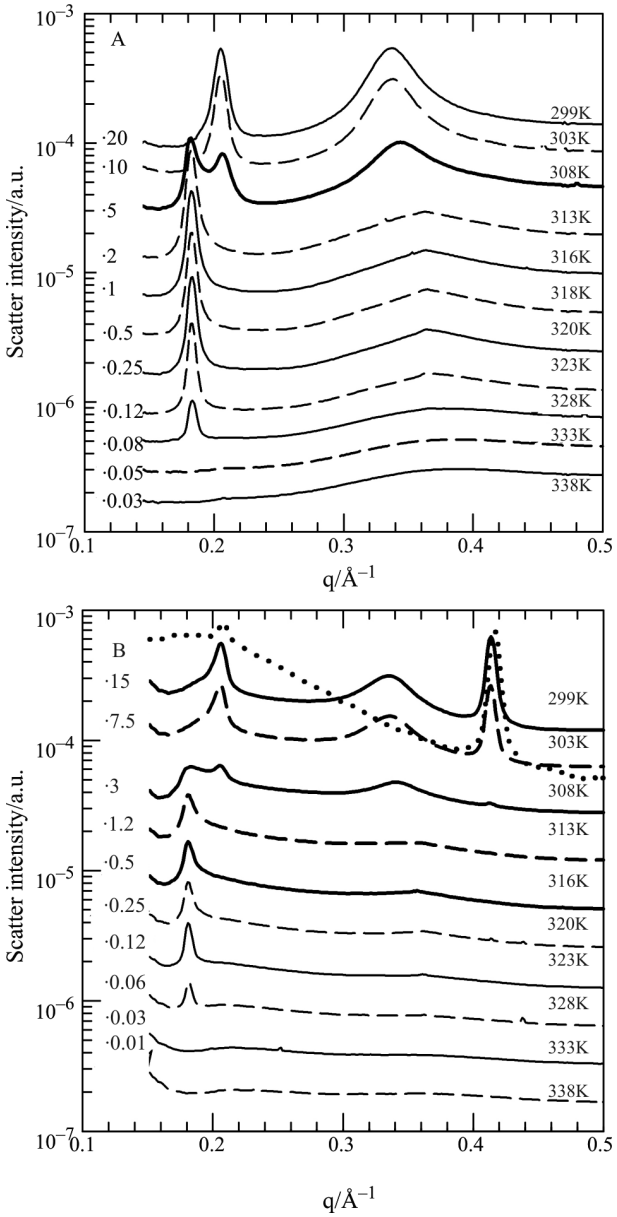

Fig. 4 SAXS profiles determined at different temperature: a – SCLC polyacrylate photopolymerised in bulk (PPOA); b – SCLC polyacrylate photopolymerised inside the aerogel (PPIA) after subtraction of the aerogel scattering background

Bragg peak (q=0.350 Å^{-1}) just visible up to 333 K, is superimposed on a diffuse peak. Two sharp signals with Bragg spacings in the ratio 1:2 in the small angle direction are typical of smectic phases. The broad diffuse scattering peak, which appears as another secondary maximum and which can be observed also in the isotropic phase, may be attributed to the underlying polymer backbone. It is known that, in the smectic phase, the main chains can preferentially occupy the space between the mesogenic layers [15] if the spacers are flexible [16], as is the case in this work (Fig. 1).

The SAXS curves obtained for the *ex-situ* nanocomposite PIA (Fig. 3b) show similar trends as observed for the bulk polymer POA. Therefore the smectic mesophase is kept after polymer confinement. Meanwhile, the smectic phase appears at a temperature lower (303 K) than in the bulk polymer POA (308 K) and the $Sm \rightarrow I$ transition occurs between 328 and 333 K instead above 338 K as observed for POA. The temperature domain of the smectic phase has approximately the same width but it is shifted to lower temperatures, in agreement with the tendency observed by DSC. Full agreement between SAXS and DSC can be only achieved by a combination of both techniques in the same experiment, as showed very well by Allais *et al*. [17].

For the photopolymerised bulk polymer (PPOA, Fig. 4a), coexistence of *K* and *Sm* phases appears more clearly than for the bulk polymer POA for the same temperature (308 K). Disappearance of the smectic phase, however, occurs at a much smaller temperature than for POA.

Figure 4b confirms the *in-situ* photopolymerisation of the monomer, yielding a smectic liquid crystal polymer inside the aerogel slice (PPIA sample). The *Sm* phase is detected above 308 K. At lower temperatures, as for the other samples, the SAXS curves of PPIA exhibit the two peaks characteristic of the crystal phase, plus an extra peak at $q \sim 0.4$ Å^{-1} matching with that observed for the monomer (dotted curve in Fig. 4b). It may therefore be concluded that the DSC peak observed at 308 K (Fig. 2a) results from monomer crystal melting. It may be assumed that this unreacted monomer is located in pores that are too narrow for polymerisation to be possible. Interestingly, a systematic investigation of monomer photopolymerisation could be helpful for a quantitative characterisation of the pore size distribution in silica aerogels.

To perform the analysis of the shape of the smectic peaks located around 0.18 Å^{-1}, the contribution of the polymer backbone must be subtracted from the measured intensity. Instead of using a model equation to fit the scattering due to the backbone conformation, a simple polynomial equation $a+bq^2+cq^4$ was used over a limited q-interval. The lower limit, q_{min}, is located above the smectic peak (around 0.24 Å^{-1}) and the upper limit, q_{max} (around 0.3 Å^{-1}), below the maximum of the diffuse peak. This equation was used for extrapolation down to low-q values and the corresponding intensities were subtracted from the experimental ones, yielding the peak plotted in Fig. 5 (filled circles). The peaks were then fitted with as follows

$$I = \frac{\sigma}{(q^2 - q_0^2)^2 + 4q_0^2\xi^{-2}} \quad (1)$$

σ corresponds to a smectic susceptibility at the ordering vector q_0 and ξ is the length of the smectic correlation. The choice of this function was made empirically, starting from a Lorentzian function, which fitted well the data around q_0. The Lorentzian function has been tested by Rappaport *et al*. [18] in order to fit a smectic peak in a low molecular nematogenic confined in a silica aerogel. However, as the whole smectic peak in this work was not well fitted by a Lorentzian, Eq. (1) is used instead. Figure 5 displays the result obtained for the line-shape analysis of the smectic peak for the PIA sample. The wave vector q_0 in Eq. (1) characterises the spacing of the smectic layers. It is related to the lamellae period d of the smectic arrangement.

The values of d extracted from the fits are plotted in Fig. 6 as a function of the reduced temperature $T_r=(T-T_{K\rightarrow SmA})/T_{K\rightarrow SmA}$. For the bulk polymer (POA) the spacing of the smectic layer slightly decreases between 36.0 and 35.3 Å with increasing temperature. Since d was determined with an accuracy of ±3%, this value roughly corresponds to the fully extended length of a side chain mesogenic unity L=35.2 Å, estimated from semi-empirical calculations [11]. Because the ratio d/L is nearly one in the mesophase, the smectic structure has a monolayer character, i.e. SmA_1. The slight decrease of d with increasing tem-

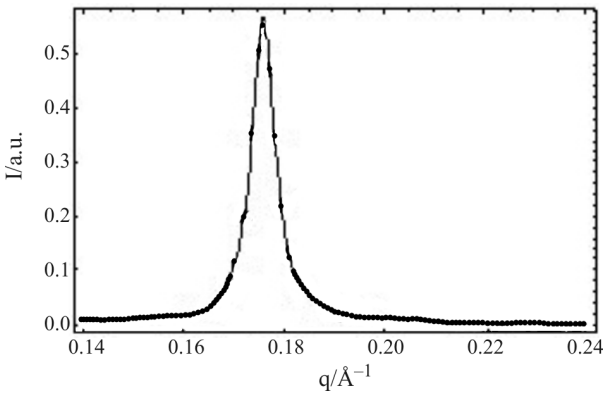

Fig. 5 Smectic peak measured at 320 K for the polymer confined in aerogel (PIA), after subtraction of the background scattering due to aerogel and polymer backbone. The solid line is a fit with Eq. (1)

perature could be due to a larger amplitude motion of the mesogenic units attached to the polymer backbone [11]. Identical results can be observed after confinement in aerogel (sample PIA). Thus, confinement has almost no effect on the smectic layer spacing *d*.

For the photopolymerised samples PPOA and PPIA (Fig. 6), the value of *d* is systematically smaller than that of samples POA and PIA. The difference, however, is small (approximately 1 Å). Thus, it may not reveal an important modification in the lamellar period and may be attributed to a higher degree of chain entanglements by photopolymerisation than by polymerisation in toluene [11]. For the bulk photopolymerised sample PPOA the temperature dependence of the spacing of the smectic layers *d* is similar to that of POA and PIA. It is not the case for PPIA that is photopolymerised in the aerogel: *d* reaches a shallow maximum at around 15 degrees above the crystalline (*K*)→smectic (*Sm*) phase transition. This feature may result from a smaller amplitude of the mesogenic fluctuations. It suggests a greater temperature stability of the lamellae that could result from building smectic layers within pores: the pore walls may hinder mesogenic fluctuations that in the bulk increase with increasing temperature. As a result, the melting temperature is shifted to a higher temperature than that of PPOA. Interestingly, the above effect of confinement is not observed for PIA, which is confined after polymerisation in solution. Thus, for the latter, it is likely that only the largest pores would be filled by polymers. For the former, monomers may fill all the pores and polymerisation will occur in pores smaller than those accessible to bulk polymers. Thus, only these smaller pores will be efficient for increasing the temperature stability of the smectic lamellae.

Figure 7 shows the variation of the correlation length ξ obtained for the four samples as a function of the temperature. The uncertainty in ξ is estimated to be ±15%. Meanwhile, ξ is related to the measured full width at half maximum (FWHM) of the peak. In order to extract the value β of FWHM that results from the smectic correlation length, the instrumental width *b* must be taken into account. For these series of measurements, *b* was close to $5.3\cdot10^{-3}$ Å^{-1}, i.e., close to the smallest FWHM measured for sample POA. Under such circumstances, unambiguous deconvolution of the peaks is difficult to achieve. In order to estimate the error on ξ due to the fact that instrumental resolution was not taken into account, Eq. (1) was used to construct a series of peaks corresponding to different ξ values, using q_0=0.1821 Å^{-1} and the FWHM B of the peaks was plotted as a function of ξ. β was deduced from *B* and *b* by means of the following relation:

$$\beta = \sqrt{\sqrt{(B^2 - b^2)}(B - b)} \qquad (2)$$

that is intermediate between the formula used for Gaussian peaks ($\beta = \sqrt{B^2 - b^2}$) and Lorentzian ones (β=*B*–*b*). For the ξ values plotted in Fig. 7 and ranging between 200 and 300 Å, the true smectic correlation length, ξ_{Sm}, is estimated to vary between 300 and 850 Å. It follows that the trend of the temperature dependence of ξ shown in Fig. 7, has a physical meaning and also that ξ_{Sm} is large enough to assess the existence of smectic organisation.

For sample POA, the value of ξ and its temperature behaviour is different from that of all other samples. As expected from the above comments, ξ remains almost constant (~360 Å) and starts to decrease on approaching the melting temperature T_I. Confinement (sample PIA) of this polymer leads to a smaller value of ξ (~ 200 Å) that begins to decrease at a lower temperature than for POA. The small value of ξ (~ 250 Å) obtained for

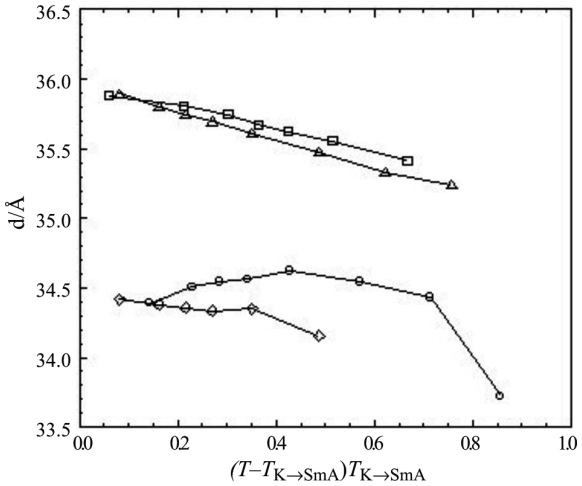

Fig. 6 Lamellae period for △ – POA, □ – PIA, ◇ – PPOA and ○ – PPIA. $T_{K–Sm}$ is the *K*→*Sm* transition temperature corresponding to each sample

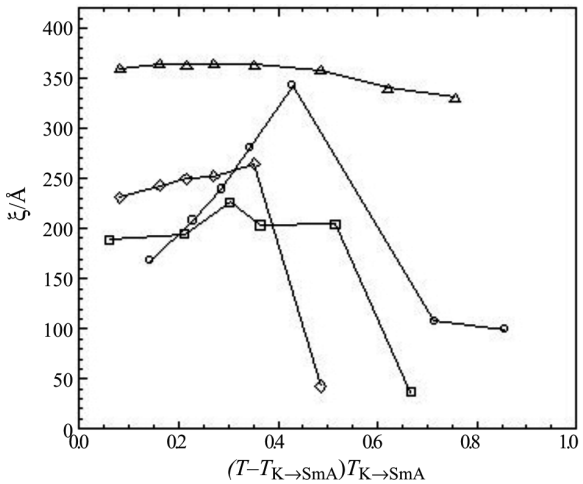

Fig. 7 Correlation lengths ξ measured for △ – POA, □ – PIA, ◇ – PPOA and ○ – PPIA. $T_{K–Sm}$ is the *K*→*Sm* transition temperature corresponding to each sample

PPOA can be attributed to the high degree of chain entanglements already mentioned. The temperature behaviour of ξ for the *in-situ* nanocomposite PPIA is again different from that of the other samples since ξ increases from a small value (~160 Å) up to nearly that observed for POA. Thus, the degree of chain entanglement will not be increased by photopolymerisation in aerogel as compared to photopolymerisation in bulk (PPOA). Hence, photopolymerisation in an aerogel allows the establishment of a stable lamellae organisation in the polymer, similar to that observed for POA. The corresponding temperature domain, however is narrow.

Conclusions

Ex-situ and *in-situ* side chain liquid crystal (SCLC) polyacrylate-silica aerogel nanocomposites were successfully prepared by infiltration of a silica aerogel with polymer and by photopolymerisation of infiltrated monomer, respectively. The main characteristics of the SmA_1 mesophase of the bulk polyacrylates are maintained for the confined polymers. Confinement shifts the temperature domain of the smectic phase to lower temperatures. The smectic ordering of the polymer confined in aerogel is short-ranged, with a correlation length that increases with increasing temperature, which is opposite to the behaviour observed for low molar mass nematogenics [18].

For the *in-situ* nanocomposite, the temperature dependence of the smectic layer spacing d as well as that of the correlation length ξ are remarkably different from that of the other samples. This feature suggests that *in-situ* polymerisation enhances the degree of order and smectic phase stability in the system.

This research is a first step for the challenge of liquid crystal polymer-aerogels composites. Knowledge about the strengths and weaknesses of this kind of systems towards applications may be achieved through confinement of liquid crystal polymers having different chemical composition and thermotropic behaviour.

Acknowledgements

The authors are grateful to the ESRF, Grenoble, for access to the French CRG beamline D2AM and the help of its technical staff, J. F. Berar, N. Boudet, B. Caillot, S. Arnaud. They acknowledge F. Bley, E. Geissler and F. Livet for stimulating discussions, Prof. Aloir A. Merlo and O. M. Ritter for synthesis and the CAPES/COFECUB program for financial support. N. P. S. thanks CAPES, Brazil, for a post-doctoral fellowship. A. R. also thanks the French society PCAS for providing the pre-polymerised TEOS precursors. H. W. Jr. acknowledges support from FAPESP and CNPq.

References

1 G. P. Crawford and S. Žumer, Liquid Crystals in Complex Geometries Formed by Polymer and Porous Networks, Taylor & Francis, London 1996.
2 T. Jin and D. Finotello, Phys. Rev. E, 69 (2004) 041704.
3 L. W. Hrubesch, J. Non-Cryst. Solids, 225 (1998) 335.
4 A. Rigacci, Thesis, École de Mines de Paris, France 1998.
5 A. Rigacci, F. Ehrburger-Dolle, E. Geissler, B. Chevalier, H. Sallée, P. Achard, O. Barbieri, S. Berthon, F. Bley, F. Livet, G. M. Pajonk, N. Pinto and C. Rochas, J. Non-Cryst. Solids, 285 (2001) 187.
6 H. Finkelmann, H. Rigsdorf and J. H. Wendorff, Macromol. Chem., 179 (1978) 273.
7 M. I. Boamfa, K. Viertler, A. Wewerka, F. Stelzer, P. C. M. Christianen and J. C. Maan, Phys. Rev. Lett., 90 (2003) 025501.
8 F. M. Aliev, Mol. Cryst. Liq. Cryst., 222 (1992) 147.
9 F. M. Aliev, Mol. Cryst. Liq. Cryst., 243 (1994) 91.
10 N. P. da Silveira, A. Rigacci, F. Ehrburger-Dolle and E. Geissler, Liquid Crystalline Polymers Confined in a Silica Aerogel: A SAXS Study. In: Fibers and Polymers Workshop, ESRF, February 11–12, 2002.
11 O. M. Ritter, A. A. Merlo, F. V. Pereira, N. P. da Silveira, E. Geissler and J. Zukerman-Schpector, Liq. Cryst., 29 (2002) 1187.
12 A. Rigacci, P. Achard, F. Ehrburger-Dolle and R. J. Pirard, J. Non-Cryst. Solids, 225 (1998) 260.
13 J. P. Simon, S. Arnaud, F. Bley, J. F. Bérar, B. Caillot, V. Comparat, E. Geissler, A. de Geyer, P. Jeantey, F. Livet and H. Okuda, J. Appl. Crystallogr., 30 (1997) 900.
14 D. J. Broer, J. Boven and N. M. Grietje, Macromol. Chem., 190 (2000) 2255.
15 L. Noirez, C. Boeffel and A. Daouad-Aladine, Phys. Rev. Lett., 80 (1998) 1453.
16 P. Davidson, Selected Topics in X-Ray Scattering by Liquid-Crystalline Polymers. In Liquid Crystals II, edited by D. M. P. Mingos, Springer Verlag, Berlin 1999, p. 1.
17 C. Allais, G. Keller, P. Lesieur, M. Ollivon and F. Artzner, J. Therm. Anal. Cal., 74 (2003) 723.
18 A. G. Rappaport, N. A. Clark, B. N. Thomas and T. Bellini, Chapter 20, p. 411 in reference 1.